Optimizing the methodology for accurate and accessible slip length measurement with atomic force microscopy

Ishida, Haruya
Department of Aeronautics and Astronautics, Kyushu University

Teshima, Hideaki
Department of Aeronautics and Astronautics, Kyushu University

Li, Qin-Yi
Department of Aeronautics and Astronautics, Kyushu University

Takahashi, Koji
Department of Aeronautics and Astronautics, Kyushu University

出版情報：International journal of thermofluids. 22, pp.100634-, 2024-05. Elsevier
バージョン：

International Journal of Thermofluids 22 (2024) 100634

Contents lists available at ScienceDirect

International Journal of Thermofluids

journal homepage: www.sciencedirect.com/journal/international-journal-of-thermofluids

Optimizing the methodology for accurate and accessible slip length measurement with atomic force microscopy

Haruya Ishida [a], Hideaki Teshima [a,b,*], Qin-Yi Li [a,b], Koji Takahashi [a,b]

[a] Department of Aeronautics and Astronautics, Kyushu University, 744 Motooka, Nishi-Ku, Fukuoka 819-0395, Japan
[b] International Institute for Carbon-Neutral Energy Research (WPI-I2CNER), Kyushu University, 744 Motooka, Nishi-Ku, Fukuoka 819-0395, Japan

ARTICLE INFO

Keywords:
Atomic force microscopy
Boundary slip
Slip length
Heat transfer
Carbon materials

ABSTRACT

The remarkable performance of cooling devices employing nano- and microscale channels has drawn considerable interest, highlighting the need for surfaces with large slip lengths to improve their efficiency. However, the large errors in slip length associated with existing techniques hinder a clear understanding of slip phenomena. In this paper, we evaluate existing analytical methods for slip length measurement with atomic force microscopy (AFM) and propose a new reliable method. We performed force curve measurements on mica, silica and highly ordered pyrolytic graphite surfaces in water using an AFM equipped with a colloidal probe. The obtained force curves were analyzed through three methods: two commonly utilized procedures, namely the recursive and intercept methods, and a novel one called the two-parameter method which we developed. Our analyses showed that the recursive method yielded slip lengths with relatively large errors, fluctuation of ±5.8 nm, which were due to inaccuracies in the cantilever's spring constant and the fluid viscosity. On the other hand, it was found that the intercept method leads to restrictions on the choice of fitting range because of the simplified formula for viscous drag. As a result, by altering the data range, the calculated slip length shows significant variations within the ranges of ±27.5 nm. The two-parameter method, unlike the standard ones, overcome these drawbacks. This method requires no pre-measured parameters, and the slip length fluctuation is independent of the fitting range and only ±3.6 nm, which is around 2/3 of that observed in the recursive method and 1/8 of that in the intercept method. Our study optimizes existing analytical protocols and offers a new way for accessible and reliable calculations of slip lengths.

1. Introduction

Despite the long-accepted boundary condition that fluids do not slip at solid-liquid interfaces, recent advances in micro- and nanoscale measurement techniques have revealed that fluids do slip [1]. This is often referred to as boundary slip and is quantitatively evaluated by the slip length, defined as the distance from the solid surface to the point where the fluid velocity linearly extrapolates to zero [2–5]. For advancing diverse fields related to fluid slippages such as molecular separation[6], osmotic power generation [7], and microchip cooling [8], research has been conducted and to date suggested multiple possible factors influencing the slip length, such as wettability [9], surface roughness [10], species [11], pH [12], surface nanobubbles [13] and surface charge [14]. Nevertheless, it remains unclear how much each factor quantitatively contributes to the slip length due to the lack of experimental efforts compared to theoretical and simulation works.

Considering the advancement and miniaturization of electronic devices, the peak heat flux has increased to a level that cannot be managed by simple air-cooling or water-cooling systems [15]. This situation requires the development of compact and efficient heat exchangers. With this background, microchannel heat exchangers, utilizing both single-phase and two-phase flows, have garnered attention due to the advantages of a large specific surface area, reduced thickness of the thermal boundary layer, and decreased thermal resistance, resulting in their superior heat transfer rates and compact designs [16]. For example, the impact of microchannel geometries and flow regimes on single-phase heat transfer characteristics has been actively studied [17, 18]. A recent experiment showed that microfluidic cooling could achieve a coefficient of performance exceeding 10^4[19] which is 10 to 100 times better than traditional systems. Efforts are also being made to miniaturize two-phase flow cooling devices like heat pipes [20], and there is active development of them thinner than 0.6 mm for cooling

* Corresponding author.
E-mail address: hteshima05@aero.kyushu-u.ac.jp (H. Teshima).

https://doi.org/10.1016/j.ijft.2024.100634

Available online 18 March 2024

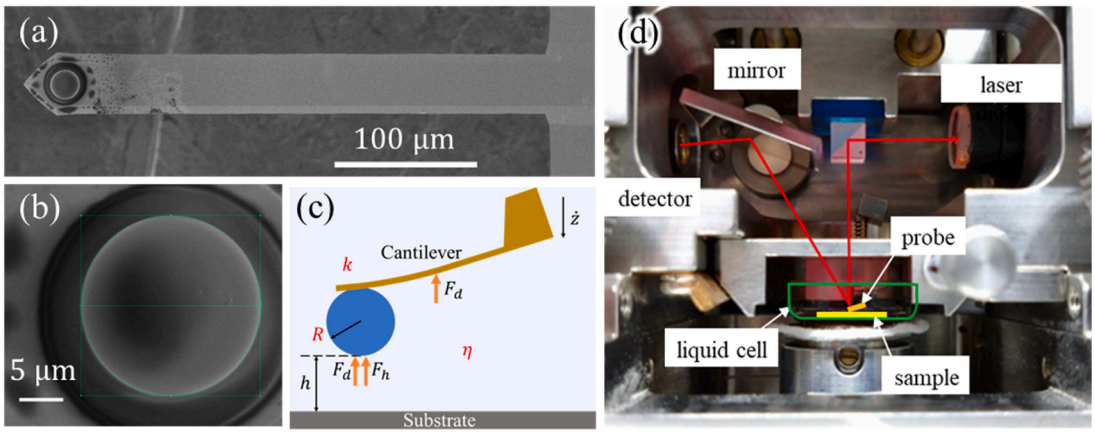

Fig. 1. Scanning electron microscope (SEM) images of (a) an AFM cantilever and (b) a microsphere attached to it. The length and width of the cantilever and the radius of the sphere were identified from these SEM images. (c) A schematic of the slip length measurement system. (d) An AFM experimental setup. The deflection of the cantilever is detected by measuring the reflected laser light from its backside. The substrate is adhered to the bottom of the liquid cell.

small and mobile devices such as tablets and smartphones [21]. However, pressure drop within the microchannel, such as those in heat sinks and the wick of the heat pipes, limits the cooling performance [22]. Considering a pipe with a constant radius$R$, a relationship between the slip length and pressure drop is expressed as follows [23]:

$$\Delta p = \frac{8\eta LQ}{\pi R^4}\left(\frac{1}{1+4b/R}\right). \quad (1)$$

Here, Δp represents the pressure drop, η the viscosity, L the length of the pipe, Q the average flow rate, R the radius, and b the slip length. For example, with R at 1000 nm and b at 100 nm, the pressure drop Δp becomes 29 % less than that under the no-slip boundary condition. Because a larger slip length results in a smaller pressure drop, employing surfaces with a larger slip length on the inner walls of microchannels is an attractive approach for enhancing the efficiency of cooling devices.

In this context, two-dimensional materials, characterized by atomic-scale thickness, smoothness, and flexibility, have garnered widespread attention. Particularly, graphene is known not only for its high thermal conductivity [24] but also its uniformity and flatness, making its surface highly slippery for fluids. Utilizing this property, water flow in the channel made from graphitic materials, such as graphene-transferred nanochannel [19,25] and carbon nanotube [26], has been extensively investigated. This slippery property is unique to graphitic materials and has not been observed in other two-dimensional materials so far including a hexagonal boron nitride [27,28], which has a similar crystalline structure, flatness and wettability to graphite. The underlying reasons for this difference remain a subject of debate. Furthermore, a recent study has reported the translucency of slip length in graphene[5], which is similar to the wetting translucency previously reported [29], indicating the potential of fluid slippage tuning by varying the number of graphene layers.

The slip length has been obtained by measuring either the velocity profiles, flow rate, or flow resistance. For example, velocity profiles near solid-liquid interfaces have been measured by fluorescence recovery after photobleaching [30–32], flow rate measurements using nanochannels [25,33], and flow resistance measurements using surface force apparatus [34,35] or AFM [2,4,5,36]. Especially, for the measurements of slip length on graphene, flow rate measurements in graphene nanochannels have been mainly utilized. However, the slip length obtained by this method represents an average over the entire channel and is highly susceptible to the effects of defects and contamination [33]. Thus, for measuring in small areas while avoiding such effects, a method with higher spatial resolution, like AFM, is preferred. The spatial resolution of slip length measurements with AFM corresponds to the radius of the sphere attached to the cantilever, typically in the tens of micrometers range.

Table. 1
A brief review of AFM slip length measurements.

Reference	Substrate	Liquid	Slip length [nm]	Method
Guriyanova, et al. [39].	Silica	Water	6	Recursive
Honig, et al. [40].	Silica	Sucrose solution	0	Intercept
Maali, et al. [41].	Mica	Water	0.7 ± 1.0	Intercept
Bonaccurso, et al. [42].	Mica	Water	8–9	Recursive
Li, et al. [43].	Graphite	Water	8	Intercept
Li, et al. [5].	Silica Graphite	Water	0.9 ± 1.2 4.3 ± 3.5	Intercept

However, the reliability of the measured slip length has become a matter of concern. Specifically, the slip length at water-graphite interfaces largely varied in the previous studies. For example, the values reported using atomic force microscopy (AFM) range from 4 to 10 nm [5,13,37,38], and the spreading values of 0–200 nm were also reported inside graphene nanochannels [33]. Chen et al. recently developed a three-dimensional flow analysis model for rectangular graphene nanochannels to accurately measure the slip length and argued the importance of a precise analysis model [25]. Therefore, for further understanding of the boundary slip conditions, the precise measurement of slip length with a rigorous analysis is essential.

In slip length measurements with AFM, the force experienced is measured as a probe with a microsphere, referred to as a colloidal probe (shown in Fig. 1(a)), approaches a flat substrate surface, as shown in Fig. 1(c). Then, the slip length is determined by analyzing the force curve. Specifically, two analysis methods have been commonly utilized: one is an exact fitting of the force curve by Vinogradova's equation [3]. Another is the estimation of slip length from the x-axis intercept of the graph that the approach velocity per viscous drag ratio is plotted against the separation between the probe tip and the target surface [44]. For simplicity, we call the former one "the recursive method" and the latter one "the intercept method" in this paper. The recursive method strictly considers the forces acting on the entire probe, whereas the parameters such as the sphere radius, spring constant and fluid viscosity need to be measured in advance. It can lead to errors in the slip length measurements because the accurate determination of the spring constant is extremely difficult [45] and the local temperature near the probe may deviate from the ambient due to the irradiation of the optical laser [46]. On the other hand, the intercept method involves certain simplifications, which enable the determination of slip length without the

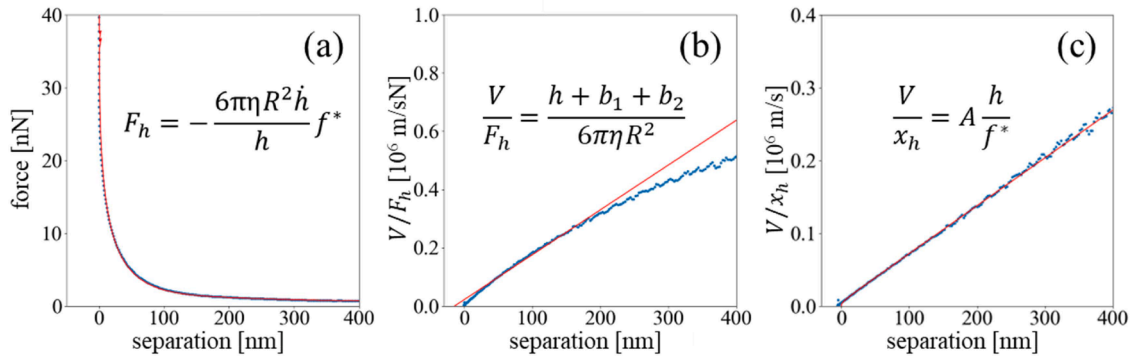

Fig. 2. Examples of fitting force curves measured on a silica surface by different methods: (a) the recursive method, (b) the intercept method, and (c) two-parameter method. (a) plots the force curve measured at 80 μm/s. (b) plots data obtained by dividing the deflection velocity calculated from the force curve measured at 80 μm/s by the same force curve. Here, only F_e is considered, and F_d is ignored. (c) is data corrected from the plot in (b) by also considering F_d.

pre-required parameters, as will be discussed later. However, errors should also arise from the simplifications themselves. Table 1 summarizes the previous reports of several slip length measurements using AFM. In prior research, slip lengths have been measured for some substrate-fluid combinations. However, some inconsistencies have been reported, for example, claims of no slip or finite slip lengths on the silica surfaces [39,40]. Such discrepancies have been often discussed in terms of factors such as determination of probe-substrate contact position and surface roughness [47], but variations in calculated slip lengths could also be due to the reliability of analytical formulas. Thus, it is necessary to evaluate the formulas themselves with respect to the effects of simplification and pre-required parameters as previously mentioned. More importantly, a novel analysis method that is not affected by these factors and has less error is highly desired.

In this study, we analyzed the same force curve data measured on mica, silica and highly ordered pyrolytic graphite (HOPG) in pure water with different methods. These three surfaces possess nano-scale flatness and are often used in slip length measurements. We found that the two commonly utilized analyses cause significant errors in the slip length due to the uncertainty in the pre-measured parameters and the arbitrariness of the fitting range. To solve these issues, we present an accurate and accessible analytical method that minimizes the error in the slip length.

2. Theory

In AFM force curve measurements, the probe detects three types of forces: F_h (viscous drag on the sphere), F_d (viscous drag on the cantilever), and F_e (electric double layer force on the sphere). F_h is described by the following equation[3]:

$$F_h = -\frac{6\pi\eta R^2 \dot{h}}{h} f^*, \tag{2}$$

where η is the viscosity, R is the radius of the sphere, and h is the distance between the sphere and the substrate (shown in Fig. 1(c)). f^* is a coefficient that describes the decrease in viscous drag owing to the boundary slip, derived by Vinogradova for two spherical surfaces[3]. Specifically, by taking the radius of one of the spheres to be infinite, the following equation is obtained.

$$f^* = -\frac{2Ah}{BC} - \frac{2h}{C-B}\left\{\frac{(B+h)(B-A)}{B^2} ln\left(1+\frac{B}{h}\right) - \frac{(C+h)(C-A)}{C^2} ln\left(1+\frac{C}{h}\right)\right\} \tag{3}$$

$$A = b_2(2+\alpha)$$

$$B = 2b_2\left(2+\alpha+\sqrt{1+\alpha+\alpha^2}\right)$$

$$C = 2b_2\left(2+\alpha-\sqrt{1+\alpha+\alpha^2}\right)$$

$$\alpha = b_1/b_2 - 1,$$

where b_1 and b_2 are the slip lengths of the sphere surface and the substrate surface, respectively. f^* is equal to 1 in the case of the no-slip boundary condition ($b_1 = b_2 = 0$), and falls between 0 and 1 when the sphere or substrate has a finite slip length. In general, the radius of a sphere attached to the cantilever is tens of micrometers [2,4,36] to detect the viscous force. The viscous drag force experienced by the cantilever F_d can be expressed as follows.

$$F_d = -6\pi\eta L_e \dot{z}, \tag{4}$$

where L_e is the effective length of the cantilever and z is the piezo position[48]. L_e can be calculated by fitting the force curve data obtained in the region where the probe and substrate are sufficiently far apart [48].

When two charged surfaces approach each other in low-ion-concentration fluids like pure water, their electric double layers overlap, resulting in a repulsive force known as the electric double layer force. It is known that an exact mathematical expression of the electric double layer force is difficult [49] because the surface charge condition alters as the surfaces come closer due to the recombination of ions [50]. Instead, the experimental data obtained by approaching the probe at low velocities (~1 μm/s) was used as F_e for the calculations.

As previously mentioned, two methods have been mainly utilized to determine the slip length from the force curves. One of them, the recursive method fits a force curve based on the force balance on the probe. The forces on the probe are balanced according to the following equation [48]:

$$F_h + F_d + F_e + F_k = 0. \tag{5}$$

Here, $F_k = kx$ represents the restorative force of the cantilever, where k is the spring constant and x is the deflection of the cantilever. By solving this equation as a recursive equation, the following equation is obtained:

$$\dot{x}_{n+1} = \frac{-k\left(x_n + \frac{1}{2}\Delta t x_n\right) - \frac{6\pi\eta R^2 \dot{z}_{n+1}}{h_{n+1}} f^* - 6\pi\eta L_e \dot{z}_{n+1} + F_e(h_{n+1})}{\frac{1}{2}k\Delta t + \frac{6\pi\eta R^2}{h_{n+1}} f^*}, \tag{6}$$

where Δt denotes the time step[48]. This equation enables the fitting of the force curve as shown in Fig. 2(a), determining the slip length. When the probe is sufficiently far from the substrate (~μm), the influence of

the slip length is minimal and F_e can be considered sufficiently small. Therefore, the initial value of x is determined by the following equation:

$$x_0 = \frac{6\pi\eta R^2 \dot{z}}{kz_0} + \frac{6\pi\eta L_e \dot{z}}{k}, \tag{7}$$

where $x_0 \ll z_0$ and $\ddot{x} \cong 0$ are assumed. In this method, the force acting on the cantilever is accurately accounted for, enabling highly precise calculations in principle. However, the necessity for the prior values of k, R, and η implies that any inaccuracies in these parameters could adversely affect the accuracy of the calculation results.

The intercept method determines the slip length by determining the intercept of V/F_h, where $V = |\dot{h}|$ is the approach velocity of the probe tip. When the slip length is considerably smaller than the probe-substrate distance ($b \ll h$), eq. (2) can be approximated as follows [44]

$$F_h = -\frac{6\pi\eta R^2 \dot{h}}{h + b_1 + b_2}. \tag{8}$$

Employing $V = |\dot{h}|$, Eq. (8) can be expressed as

$$\frac{V}{F_h} = \frac{h + b_1 + b_2}{6\pi\eta R^2}. \tag{9}$$

Because V/F_h is proportional to $h + b_1 + b_2$, the slip length is determined by its intercept on the x-axis as shown in Fig. 2(b). Here, the influence of F_e is eliminated by subtracting the experimentally measured F_e from the experimental data. This method has the advantage of being able to calculate slip length without the values of η and R. However, it is important to note that this method relies on the approximation where $b \ll h$ and disregards F_d, which could potentially lead to discrepancies between the measurement data and the equation.

We propose a new analytical method, named "two-parameter method," to overcome the limitations mentioned above. This approach involves transforming eq. (2) into the following form:

$$\frac{V}{x_h} = A\frac{h}{f^*}, \tag{10}$$

where $x_h = F_h/k$ is the component of deflection due to the viscous drag on the sphere F_h and $A = k/6\pi\eta R^2$. Furthermore, we subtracted not only F_e but also F_d from the experimental data to address the issue of ignoring F_d in the intercept method. In this new approach, the parameter A and the slip length b_2 in f^* are used as two fitting parameters. This method addresses the necessity of prior knowledge of the parameters faced by the recursive method, as well as the issue of discrepancies between the equation and measured data in the intercept method. As a result, as shown in Fig. 2(c), the entire force curve fits well despite knowing the parameters in advance. It should be noted that the slip length of the sphere surface was measured to be $b_1 = 5.0$ nm which is determined using Eq. (10), under the assumption that it is identical to that of the silica substrate surface[48].

3. Materials and methods

Colloidal probes were fabricated by attaching a silica sphere (microParticles, GmbH) to the tipless cantilever (MikroMasch, HQ:CSC37/tipless/Cr-Au) with an adhesive (Epoxy Technology, EPO-TEK 353ND). In this study, two probes were used. Probe 1 was utilized for measurements on mica, while Probe 2 was employed for measurements on silica and HOPG surfaces. The spring constants were determined using the thermal noise method to be 0.36 N/m and 0.31 N/m for Probe 1 and 2, respectively. The dimensions of the cantilevers and the radii of the spheres for probes 1 and 2 were measured from the scanning electron microscope images, as shown in Fig. 1(a, b). For Probe 1, the length, width, and radius of the sphere were measured to be 370.7 μm, 39.4 μm, and 10.1 μm, respectively. For Probe 2, these were 370.2 μm for length, 41.6 μm for width, and 10.2 μm for the radius of the sphere. The cut-out

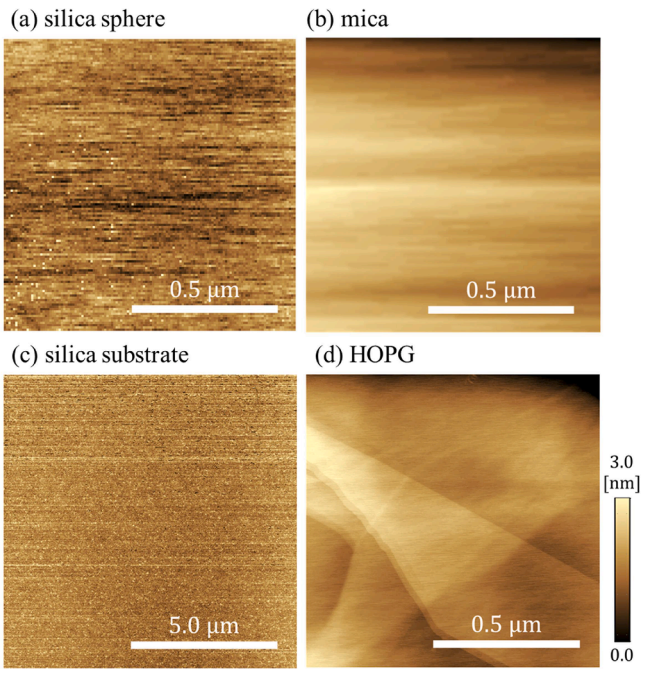

Fig. 3. AFM surface topography of (a) a silica sphere attached to the cantilever, where the surface shape of the sphere was flattened by a spherical fitting, (b) a mica surface, (c) a silica surface, and (d) an HOPG surface, respectively. The surface roughness was measured as R_a values of (a) 0.45 nm, (b) 0.29 nm, (c) 0.29 nm, and (d) 0.35 nm, respectively.

silica substrate was cleaned by ultrasonication in acetone for 30 min. The liquid cells for the measurements were fabricated by attaching the bare mica substrate, silica substrate and HOPG (Alliance Biosystems, SPI-1 Grade) substrates to the bottom of the cells. We chose those surfaces in order to compare surfaces with almost no slip (mica), intermediate slip (silica) and a large slip (HOPG). The colloidal probe and silica substrate were cleaned and hydrophilized by atmospheric plasma treatment (VACUUM DEVICE, PIB-10) before usage to keep the surface conditions constant. As shown in Fig. 3, the sphere surface and three substrate surfaces were nanoscopically flat. In this study, deionized water (RFP742HA, Advantec, Japan) was chosen as the target liquid because of its importance for a variety of scientific and industrial fields. Investigating the use of other solutions, for example, refrigerants and nonpolar solvents, as well as examining temperature dependencies, would be an intriguing research topic; however, it is beyond the scope of this study.

Force curve measurements were performed using an AFM (Shimadzu Corp., SPM-8100FM). The sum of the F_h, F_d and F_e was measured at an approach velocity of 80 μm/s. As discussed in Section 2, in parts of the force curve where the distance between the probe and the substrate is sufficiently large, F_h and F_e become so small that they can be ignored. Therefore, we calculated L_e from the values of F_d measured at distances greater than 1 μm between the probe and the substrate and L_e was determined to be 292.7 μm for probe 1 361.9 μm for probe 2. Only F_e was measured at an approach velocity of 1 μm/s. At an approach velocity of 1 μm/s, only F_e is measured because the viscous drags F_h and F_d, which are proportional to velocity, can be neglected. In the intercept method and two-parameter method, the influence of the electric double-layer force is eliminated by subtracting the data measured at 1 μm/s from the data obtained at 80 μm/s. Before starting the experiment, we waited for over two hours to allow the temperature to reach a steady state. The water temperature was monitored using a thermocouple and was stable at 24.0 °C during measurements on mica, 26.4 °C on silica, and 30.7 °C on HOPG, which was approximately 3–6 °C higher than room temperature. The accuracy of the thermocouple was ±0.5 °C, and the resolution was

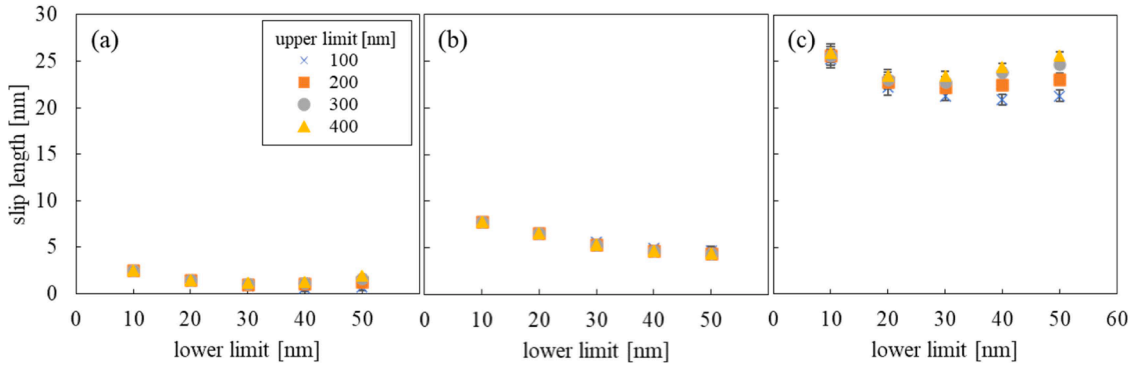

Fig. 4. Slip lengths calculated using the recursive method. The fitting was performed using data ranges with lower limits of 10–50 nm and upper limits of 100–400 nm. (a) displays results obtained on a mica surface, while (b) and (c) show those on a silica and HOPG surface, respectively. The viscosities were (a) 0.91 mPa · s, (b) 0.86 mPa · s, (c) 0.79 mPa · s, respectively. Error bars represent the standard error calculated from 16 measurements.

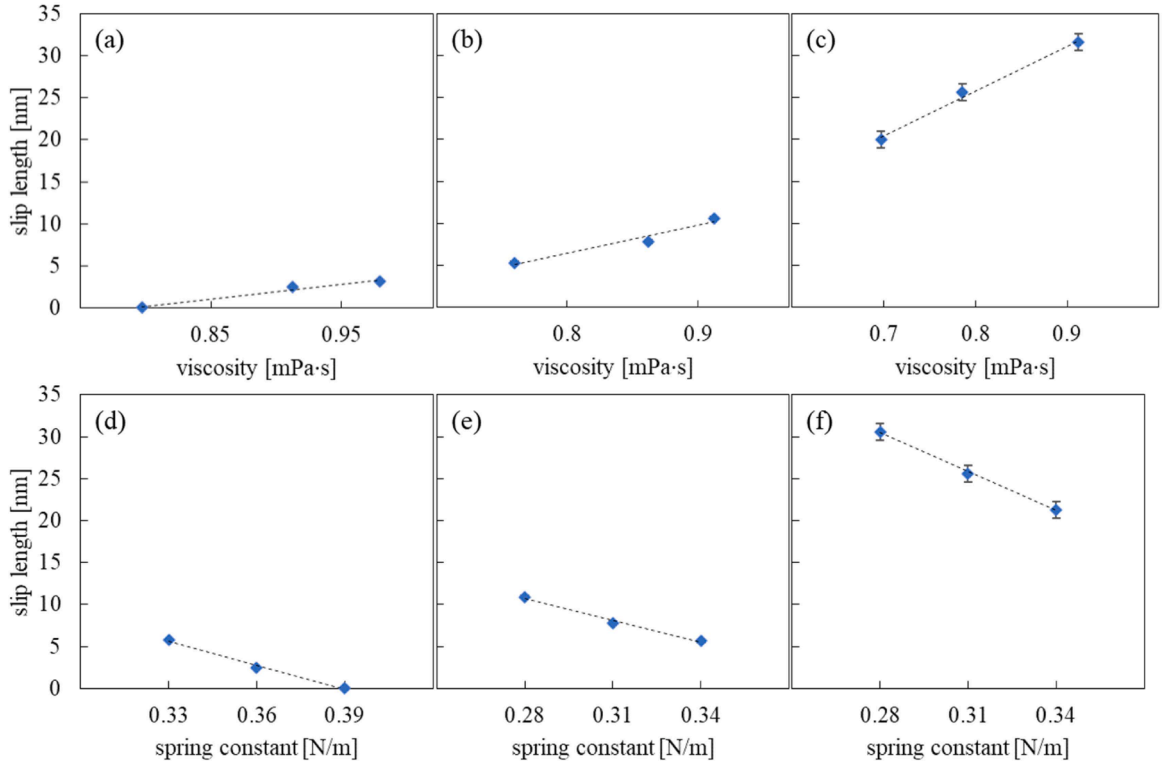

Fig. 5. The impact of errors in spring constant and viscosity on slip length. Results are shown for (a)(d) on mica, (b)(e) on silica, and (c)(f) on HOPG surfaces. In (a)(b)(c), the spring constant was varied within a range of ±8 %, and the viscosity was fixed at 0.91 mPa · s for mica, 0.86 mPa · s for silica, and 0.79 mPa · s for HOPG. In (d)(e)(f), three types of viscosities corresponding to room temperature, the measured temperature, and the measured temperature +6 °C were used. For example, they are 24.0 °C, 30.7 °C, and 36.7 °C for HOPG. The spring constant was fixed at 0.36 N/m for mica and 0.31 N/m for silica and HOPG. Since the impact of the data range is minimal, the data range was calculated as 10–200 nm as a representative.

0.1 °C. This temperature variation may be due to the difference in absorbance and thermal conductivity of the solid materials. Each measurement was conducted in about 8 min, during which time the thermocouple did not detect any temperature changes. This means that the temperature change during the experiment was less than 0.1 °C. Therefore, it can be considered that the experimental system was isothermal. We note that the local temperature near the probe tip should be much higher due to the irradiation of the optical laser [46]. Additionally, during measurements, the water in the liquid cell was exposed to the atmosphere, so it is necessary to be aware that evaporation continuously occurred. In this study, there was still enough water left in the liquid cell after the experiments, indicating that the evaporation was mild. In the case of electrolyte solutions, evaporation could increase the concentration, thus changing the viscosity [51]; however, such an effect was not present in this study as pure water was used.

4. Results and discussion

4.1. Recursive method

The calculated slip length using the recursive method is shown in Fig. 4. The fitting range was varied between lower limits of 10–50 nm and upper limits of 100–400 nm. It was found that the slip lengths do not depend on the fitting range. This is because the recursive method considers all the forces acting on the cantilever without any simplifications. Therefore, in the range where water can be considered as a continuum

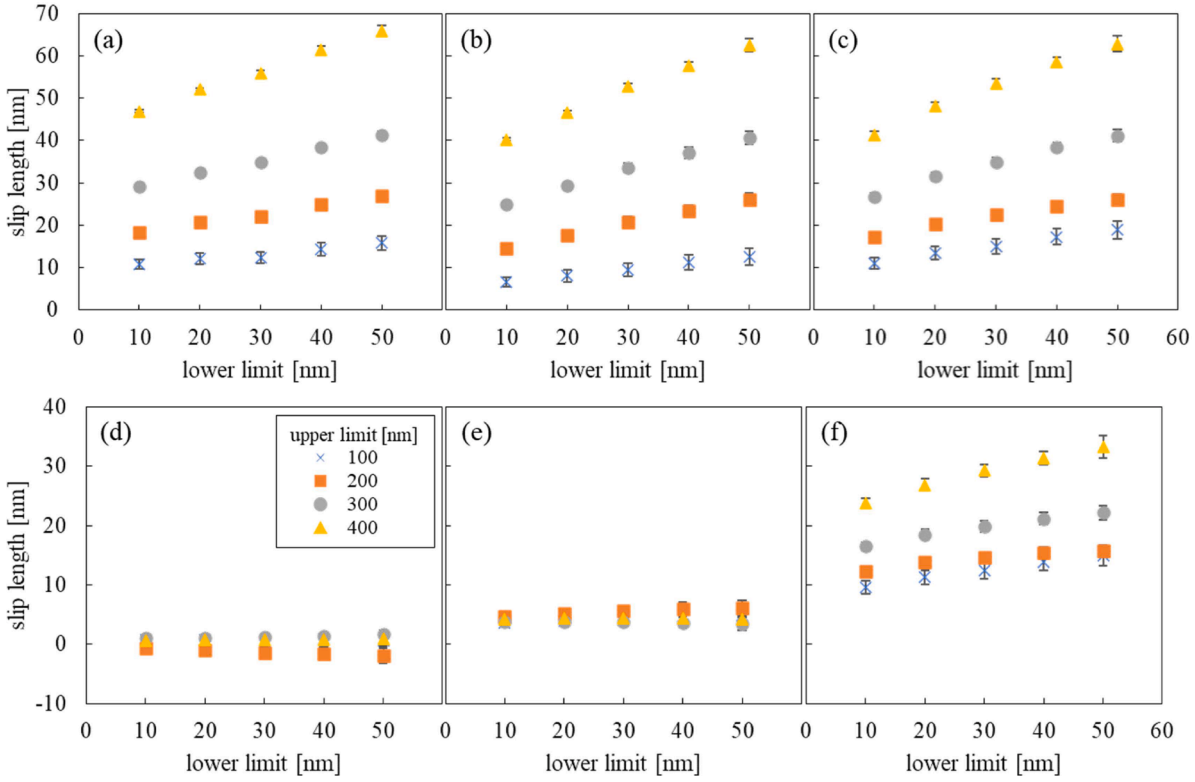

Fig. 6. Slip lengths calculated using the intercept method. The lower and upper limits were varied with 10–50 nm and 100–400 nm, respectively. (a), (b) and (c) depict results of the normal intercept method, while (d), (e) and (f) take into consideration the effect of F_d. (a) and (d) display results obtained on a mica surface, while (b) and (e) show those on a silica surface, and (c) and (f) are on an HOPG surface.

(higher than 1 nm[52]), the measured data and fitting curves agree well over the entire range, which is an advantage of the recursive method.

In Fig. 5(a, b, c), the spring constant was varied by ±8 %, which corresponds to the error in the thermal noise method reported in a previous study [53]. In Fig. 5(d, e, f), three types of viscosities corresponding to room temperature, the temperature measured by a thermocouple, and the thermocouple's temperature +6 °C were selected. This is because the temperature near the tip of the probe has been reported to be 6 °C higher than the surrounding liquid temperature due to the laser irradiation [33]. It should be noted that the temperature increase due to the laser irradiation should depend on the intensity of the laser and material of the probe and coating film and thus can be much higher than 6 °C. Here, the fitting range between 10 and 200 nm was chosen as a reference. The calculated slip lengths yielded a range of 0–3.1 nm for mica, 5.3–10.6 nm for silica and 20.0–31.6 nm for HOPG due to viscosity variations, and 0–5.8 nm for mica, 5.6–10.9 nm for silica and 21.3–30.6 nm for HOPG due to spring constant errors. Thus, using this method, the slip length varied by up to ±5.8 nm and ±4.6 nm due to the errors in viscosity and spring constant, respectively. The results demonstrate that the unavoidable errors in the parameters can lead to significant errors in the calculated slip length. It is especially important to note that the combined effect of errors in each parameter can produce larger errors.

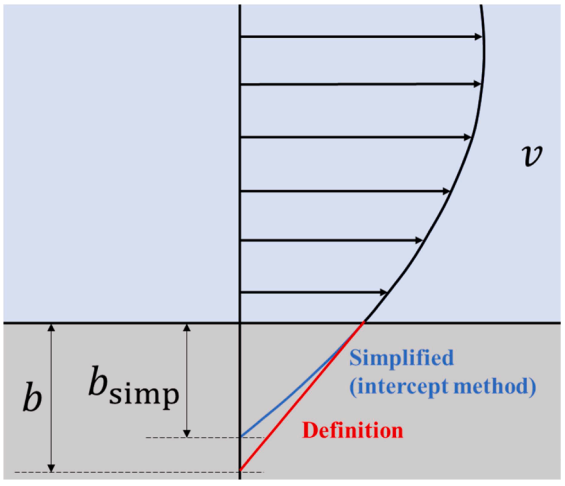

Fig. 7. A schematic illustrating the velocity distribution of fluid near a solid-liquid interface. The red line represents a linear extrapolation of fluid velocity based on the definition of slip length, while the blue curve shows a parabolic extrapolation resulting from the approximation of $b \ll h$. Here, b denotes the exact slip length and b_{simp} represents the simplified slip length.

4.2. Intercept method

The results of the slip length calculations using the normal intercept method are shown in Fig. 6(a, b, c). The values were strongly dependent on both the lower and upper limits, varying within the range of 10.9–65.8 nm for mica, 6.6–62.6 nm for the silica and 11.0–62.8 nm for the HOPG. The variation in slip length calculated by this method reached a maximum of ±27.5 nm. It was observed that an increase in both the upper and lower limits corresponded to larger slip lengths. This trend was consistent across the measurements. This should be attributed to the simplifications made to derive eq. (8), specifically the neglect of F_d and the assumption that $b \ll h$.

First, we consider the neglect of F_d. F_d can be disregarded when F_d is considerably smaller than F_h, corresponding to the case where h is small. This is expressed as follows:

$$\frac{F_d}{F_h} = \frac{L_e h}{R^2 f^*} \ll 1. \tag{11}$$

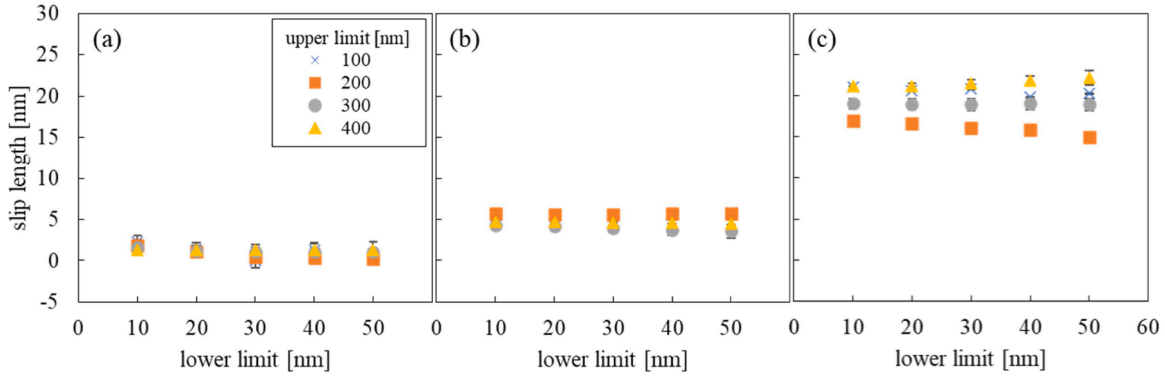

Fig. 8. Slip lengths calculated using two-parameter method. The lower and upper limits were varied with 10–50 nm and 100–400 nm, respectively. (a), (b) and (c) are the results for mica, silica and HOPG surfaces, respectively.

Transforming eq. (11) yields the following condition for h:

$$h \ll \frac{R^2 f^*}{L_e} < \frac{R^2}{L_e}. \tag{12}$$

As previously mentioned, in this study, R and L_e were 10.1 μm and 292.7 μm for probe 1 and 10.2 μm and 361.9 μm for probe 2, respectively. Consequently, eq. (12) gives $h \ll 348.5$nm for probe 1 and $h \ll 287.4$nm for probe 2, which indicates the upper limit should be much smaller than these values in this study. This limitation can be addressed by subtracting F_d from the force curve to isolate F_h. The results are displayed in Fig. 6(d, e, f), which show less dependency of the calculated slip length on the upper limit.

Next, we discuss the approximation of $b \ll h$. While the slip lengths on the mica and silica surface showed no dependence on the lower limit after the consideration of F_d (Fig. 6(d, e)), a significant dependency was still observed for the HOPG surface as shown in Fig. 6(f). This is because of a simplified representation of slip length induced by the approximation, as shown in Fig. 7. The exact slip length b is defined by linear interpolation of the velocity distribution, whereas the simplified slip length in eq. (8) corresponds to b_{simp}, which is a parabolic interpolation of the velocity distribution. The difference between b and b_{simp} depends on the ratio of the actual slip length b to the probe-substrate distance h. When b is much smaller than h, the difference between b and b_{simp} is small enough to ignore. If $b \ll h$ is not satisfied, the difference becomes pronounced. Therefore, because the graphite surface has a large slip length, the slip length calculated by the intercept method varies depending on the lower limit as shown in Fig. 6(f). Therefore, although the intercept method has the advantage of not being affected by errors in spring constant or viscosity, it should not be used for surfaces that are expected to have a large slip length, such as graphite and hydrophobic surfaces.

4.3. Two-parameter method

As shown in Fig. 8, the slip length calculated with two-parameter method showed minimal variations, range of 0–2.3 nm for mica, 3.6–5.9 nm for silica and 15.0–22.1 nm for HOPG, and did not show any dependency on the fitting ranges. The variation in slip length was at most ±3.6 nm which represents the smallest variation among the three methods. The value of $A = k/6\pi\eta R^2$, obtained through fitting, was found to be 2.10×10^{11} $(\mathrm{m} \cdot \mathrm{s})^{-1}$ for mica, 2.07×10^{11} $(\mathrm{m} \cdot \mathrm{s})^{-1}$ for silica and 2.25×10^{11} $(\mathrm{m} \cdot \mathrm{s})^{-1}$ for HOPG. These values showed good agreement with the calculated values based on pre-measured data: $2.06 \times 10^{11}(\mathrm{m} \cdot \mathrm{s})^{-1}$ for mica, $1.84 \times 10^{11}(\mathrm{m} \cdot \mathrm{s})^{-1}$ for silica, and $2.00 \times 10^{11}(\mathrm{m} \cdot \mathrm{s})^{-1}$ for HOPG. The slight variation in A falls within the error range of the spring constant and viscosity, indicating that the values obtained by the fitting are reasonable. Also, these slip lengths are within the ranges obtained by the recursive and intercept methods, confirming their consistency. Therefore, it is obvious that this new analysis is the most accessible and reliable method for measuring slip length with AFM.

5. Conclusion

To conclude, we analyzed force curve data by three different methods: the recursive method, the intercept method, and the two-parameter method we newly proposed. The recursive method was found to induce errors in the slip length due to the uncertainty of the pre-measured parameters. Although the maximum fluctuations of slip length induced by the variations in the viscosity and spring constant were recorded at ±5.8 nm and ±4.6 nm, respectively, it is important to note that the synergetic effects of these factors can lead to larger errors. Furthermore, we revealed that the choice of fitting range significantly impacts the slip length calculations in the intercept method. The fluctuation in slip length was up to ±27.5 nm. Though we successfully eliminated the regulation of the upper limit by isolating F_h from the force curve, the lower limit needed to meet the condition$b \ll h$. Thus, we concluded that the intercept method is not suitable for substrates with large slip lengths. Two-parameter method addressed the issues of previous methods, significantly minimizing the error of slip length. In our experiments, the error in slip length was reduced to a mere ±3.6 nm, which was at most 8 times lower than the values calculated by the conventional methods. These results significantly improved the accuracy of AFM-based slip length measurements and will be valuable for the development of nanofluidic devices utilizing the slippery properties of carbon-based two-dimensional materials.

CRediT authorship contribution statement

Haruya Ishida: Writing – original draft, Visualization, Validation, Software, Methodology, Investigation, Formal analysis, Conceptualization. **Hideaki Teshima:** Writing – review & editing, Supervision, Resources, Project administration, Methodology, Investigation, Funding acquisition, Conceptualization. **Qin-Yi Li:** Writing – review & editing, Supervision, Conceptualization. **Koji Takahashi:** Writing – review & editing, Supervision, Funding acquisition, Conceptualization.

Declaration of competing interest

The authors declare that they have no known competing financial interests or personal relationships that could have appeared to influence the work reported in this paper.

Data availability

Data will be made available on request.

Acknowledgements

We thank Prof. Xuehua Zhang at the University of Alberta for the fruitful discussion.

Funding

This work was supported by JST CREST Grant No. JPMJCR18I1 and PRESTO Grant No. JPMJPR23O8, and JSPS KAKENHI Grant Nos. JP20H02089, JP22KK0249, JP22K14193, and JP22K18772.

References

[1] C. Neto, D.R. Evans, E. Bonaccurso, H.-J. Butt, V.S.J. Craig, Boundary slip in Newtonian liquids: a review of experimental studies, Rep. Prog. Phys. 68 (2005) 2859, https://doi.org/10.1088/0034-4885/68/12/R05.
[2] D. Jing, B. Bhushan, Boundary slip of superoleophilic, oleophobic, and superoleophobic surfaces immersed in deionized water, hexadecane, and ethylene glycol, Langmuir 29 (2013) 14691–14700, https://doi.org/10.1021/la4030876.
[3] O.I. Vinogradova, Drainage of a thin liquid film confined between hydrophobic surfaces, Langmuir 11 (1995) 2213–2220, https://doi.org/10.1021/la00006a059.
[4] L. Zhu, P. Attard, C. Neto, Reconciling slip measurements in symmetric and asymmetric systems, Langmuir 28 (2012) 7768–7774, https://doi.org/10.1021/la301040d.
[5] H. Li, Z. Xu, C. Ma, M. Ma, Translucency and negative temperature-dependence for the slip length of water on graphene, Nanoscale 14 (2022) 14636–14644, https://doi.org/10.1039/d2nr01481e.
[6] H.B. Park, J. Kamcev, L.M. Robeson, M. Elimelech, B.D. Freeman, Maximizing the right stuff: the trade-off between membrane permeability and selectivity, Science 356 (2017) eaab0530, https://doi.org/10.1126/science.aab0530.
[7] A. Siria, P. Poncharal, A.-L. Biance, R. Fulcrand, X. Blase, S.T. Purcell, L. Bocquet, Giant osmotic energy conversion measured in a single transmembrane boron nitride nanotube, Nature 494 (2013) 455–458, https://doi.org/10.1038/nature11876.
[8] H.B. Bacha, N. Ullah, A. Hamid, N.A. Shah, A comprehensive review on nanofluids: synthesis, cutting-edge applications, and future prospects, Int. J. Thermofluids 22 (2024) 100595, https://doi.org/10.1016/j.ijft.2024.100595.
[9] C. Sendner, D. Horinek, L. Bocquet, R.R. Netz, Interfacial water at hydrophobic and hydrophilic surfaces: slip, viscosity, and diffusion, Langmuir 25 (2009) 10768–10781, https://doi.org/10.1021/la901314b.
[10] T. Lee, E. Charrault, C. Neto, Interfacial slip on rough, patterned and soft surfaces: a review of experiments and simulations, Adv. Colloid Interface Sci. 210 (2014) 21–38, https://doi.org/10.1016/j.cis.2014.02.015.
[11] V.S. Craig, C. Neto, D.R. Williams, Shear-dependent boundary slip in an aqueous Newtonian liquid, Phys. Rev. Lett. 87 (2001) 054504, https://doi.org/10.1103/PhysRevLett.87.054504.
[12] P. Tian, Y. Li, Effect of pH on effective slip length and surface charge at solid-oil interfaces of roughness-induced surfaces, Micromachines (Basel) 12 (2021) 752, https://doi.org/10.3390/mi12070752.
[13] Y.-H. Lu, C.-W. Yang, I.-S. Hwang, Molecular layer of gaslike domains at a hydrophobic–water interface observed by frequency-modulation atomic force microscopy, Langmuir 28 (2012) 12691–12695, https://doi.org/10.1021/la301671a.
[14] Y. Pan, B. Bhushan, Role of surface charge on boundary slip in fluid flow, J. Colloid Interface Sci. 392 (2013) 117–121, https://doi.org/10.1016/j.jcis.2012.10.043.
[15] M. Asadi, G. Xie, B. Sunden, A review of heat transfer and pressure drop characteristics of single and two-phase microchannels, Int. J. Heat Mass Transf. 79 (2014) 34–53, https://doi.org/10.1016/j.ijheatmasstransfer.2014.07.090.
[16] K. El Kadi, F. Alnaimat, S.A. Sherif, Recent advances in condensation heat transfer in mini and micro channels: a comprehensive review, Appl. Therm. Eng. 197 (2021) 117412, https://doi.org/10.1016/j.applthermaleng.2021.117412.
[17] Y. Alihosseini, M. Zabetian Targhi, M.M. Heyhat, N. Ghorbani, Effect of a micro heat sink geometric design on thermo-hydraulic performance: a review, Appl. Therm. Eng. 170 (2020) 114974, https://doi.org/10.1016/j.applthermaleng.2020.114974.
[18] A. Moradikazerouni, M. Afrand, J. Alsarraf, O. Mahian, S. Wongwises, M.-D. Tran, Comparison of the effect of five different entrance channel shapes of a micro-channel heat sink in forced convection with application to cooling a supercomputer circuit board, Appl. Therm. Eng. 150 (2019) 1078–1089, https://doi.org/10.1016/j.applthermaleng.2019.01.051.
[19] K.-T. Chen, Q.-Y. Li, K. Takahashi, Slip flow on graphene: current status and perspective, J. Therm. Sci. 31 (2022) 1115–1134, https://doi.org/10.1007/s11630-022-1668-8.
[20] X. Chen, H. Ye, X. Fan, T. Ren, G. Zhang, A review of small heat pipes for electronics, Appl. Therm. Eng. 96 (2016) 1–17, https://doi.org/10.1016/j.applthermaleng.2015.11.048.
[21] H. Tang, Y. Tang, Z. Wan, J. Li, W. Yuan, L. Lu, Y. Li, K. Tang, Review of applications and developments of ultra-thin micro heat pipes for electronic cooling, Appl. Energy 223 (2018) 383–400, https://doi.org/10.1016/j.apenergy.2018.04.072.
[22] Y. Sui, C.J. Teo, P.S. Lee, Y.T. Chew, C. Shu, Fluid flow and heat transfer in wavy microchannels, Int. J. Heat Mass Transf. 53 (2010) 2760–2772, https://doi.org/10.1016/j.ijheatmasstransfer.2010.02.022.
[23] C. Vega-Sánchez, C. Neto, Pressure drop measurements in microfluidic devices: a review on the accurate quantification of interfacial slip, Adv. Mater. Interfaces 9 (2022) 2101641, https://doi.org/10.1002/admi.202101641.
[24] S. Ghosh, I. Calizo, D. Teweldebrhan, E.P. Pokatilov, D.L. Nika, A.A. Balandin, W. Bao, F. Miao, C.N. Lau, Extremely high thermal conductivity of graphene: prospects for thermal management applications in nanoelectronic circuits, Appl. Phys. Lett. 92 (2008) 151911, https://doi.org/10.1063/1.2907977.
[25] K.-T. Chen, Q.-Y. Li, T. Omori, Y. Yamaguchi, T. Ikuta, K. Takahashi, Slip length measurement in rectangular graphene nanochannels with a 3D flow analysis, Carbon N. Y. 189 (2022) 162–172, https://doi.org/10.1016/j.carbon.2021.12.048.
[26] K. Falk, F. Sedlmeier, L. Joly, R.R. Netz, L. Bocquet, Molecular origin of fast water transport in carbon nanotube membranes: superlubricity versus curvature dependent friction, Nano Lett. 10 (2010) 4067–4073, https://doi.org/10.1021/nl1021046.
[27] A. Keerthi, S. Goutham, Y. You, P. Iamprasertkun, R.A.W. Dryfe, A.K. Geim, B. Radha, Water friction in nanofluidic channels made from two-dimensional crystals, Nat. Commun. 12 (2021) 3092, https://doi.org/10.1038/s41467-021-23325-3.
[28] G. Tocci, L. Joly, A. Michaelides, Friction of water on graphene and hexagonal boron nitride from ab initio methods: very different slippage despite very similar interface structures, Nano Lett 14 (2014) 6872–6877, https://doi.org/10.1021/nl502837d.
[29] C.-J. Shih, M.S. Strano, D. Blankschtein, Wetting translucency of graphene, Nat. Mater. 12 (2013) 866–869, https://doi.org/10.1038/nmat3760.
[30] R. Pit, H. Hervet, L. Léger, Friction and slip of a simple liquid at a solid surface, Tribol. Lett. 7 (1999) 147–152, https://doi.org/10.1023/a:1019161101812.
[31] K.B. Migler, H. Hervet, L. Leger, Slip transition of a polymer melt under shear stress, Phys. Rev. Lett. 70 (1993) 287–290, https://doi.org/10.1103/PhysRevLett.70.287.
[32] R. Pit, H. Hervet, L. Leger, Direct experimental evidence of slip in hexadecane: solid interfaces, Phys. Rev. Lett. 85 (2000) 980–983, https://doi.org/10.1103/PhysRevLett.85.980.
[33] Q. Xie, M.A. Alibakhshi, S. Jiao, Z. Xu, M. Hempel, J. Kong, H.G. Park, C. Duan, Fast water transport in graphene nanofluidic channels, Nat. Nanotechnol. 13 (2018) 238–245, https://doi.org/10.1038/s41565-017-0031-9.
[34] B. Cross, C. Barraud, C. Picard, L. Léger, F. Restagno, É. Charlaix, Wall slip of complex fluids: interfacial friction versus slip length, Phys. Rev. Fluids 3 (2018) 062001, https://doi.org/10.1103/PhysRevFluids.3.062001.
[35] J. Baudry, E. Charlaix, A. Tonck, D. Mazuyer, Experimental evidence for a large slip effect at a nonwetting Fluid−Solid interface, Langmuir 17 (2001) 5232–5236, https://doi.org/10.1021/la0009994.
[36] G. Greenwood, J.M. Kim, Q. Zheng, S.M. Nahid, S. Nam, R.M. Espinosa-Marzal, Effects of Layering and Supporting Substrate on Liquid Slip at the Single-Layer Graphene Interface, ACS Nano 15 (2021) 10095–10106, https://doi.org/10.1021/acsnano.1c01884.
[37] D.Y. Li, D.L. Jing, Y.L. Pan, K. Ahmad, X.Z. Zhao, Slip length measurement of water flow on graphite surface using atomic force microscope, Adv. Mat. Res. 941–944 (2014) 1581–1584, https://doi.org/10.4028/www.scientific.net/amr.941-944.1581.
[38] A. Maali, T. Cohen-Bouhacina, H. Kellay, Measurement of the slip length of water flow on graphite surface, Appl. Phys. Lett. 92 (2008) 053101, https://doi.org/10.1063/1.2840717.
[39] S. Guriyanova, B. Semin, T.S. Rodrigues, H.-J. Butt, E. Bonaccurso, Hydrodynamic drainage force in a highly confined geometry: role of surface roughness on different length scales, Microfluid. Nanofluidics 8 (2010) 653–663, https://doi.org/10.1007/s10404-009-0498-2.
[40] C.D.F. Honig, W.A. Ducker, No-slip hydrodynamic boundary condition for hydrophilic particles, Phys. Rev. Lett. 98 (2007) 028305, https://doi.org/10.1103/PhysRevLett.98.028305.
[41] A. Maali, Y. Wang, B. Bhushan, Evidence of the no-slip boundary condition of water flow between hydrophilic surfaces using atomic force microscopy, Langmuir 25 (2009) 12002–12005, https://doi.org/10.1021/la902934j.
[42] E. Bonaccurso, M. Kappl, H.-J. Butt, Hydrodynamic force measurements: boundary slip of water on hydrophilic surfaces and electrokinetic effects, Phys. Rev. Lett. 88 (2002) 076103, https://doi.org/10.1103/PhysRevLett.88.076103.
[43] D. Li, Y. Wang, Y. Pan, X. Zhao, Measurements of slip length for flows over graphite surface with gas domains, Appl. Phys. Lett. 109 (2016) 151602, https://doi.org/10.1063/1.4964437.
[44] C. Cottin-Bizonne, B. Cross, A. Steinberger, E. Charlaix, Boundary slip on smooth hydrophobic surfaces: intrinsic effects and possible artifacts, Phys. Rev. Lett. 94 (2005) 056102, https://doi.org/10.1103/PhysRevLett.94.056102.
[45] R. Li, H. Ye, W. Zhang, G. Ma, Y. Su, An analytic model for accurate spring constant calibration of rectangular atomic force microscope cantilevers, Sci. Rep. 5 (2015) 15828, https://doi.org/10.1038/srep15828.
[46] J. te Riet, A.J. Katan, C. Rankl, S.W. Stahl, A.M. van Buul, I.Y. Phang, A. Gomez-Casado, P. Schön, J.W. Gerritsen, A. Cambi, A.E. Rowan, G.J. Vancso, P. Jonkheijm, J. Huskens, T.H. Oosterkamp, H. Gaub, P. Hinterdorfer, C.G. Figdor, S. Speller, Interlaboratory round robin on cantilever calibration for AFM force spectroscopy, Ultramicroscopy 111 (2011) 1659–1669, https://doi.org/10.1016/j.ultramic.2011.09.012.
[47] C.D.F. Honig, W.A. Ducker, Squeeze film lubrication in silicone oil: experimental test of the no-slip boundary condition at solid−liquid interfaces, J. Phys. Chem. C 112 (2008) 17324–17330, https://doi.org/10.1021/jp804736a.

[48] L. Zhu, P. Attard, C. Neto, Reliable measurements of interfacial slip by colloid probe atomic force microscopy. I. Mathematical modeling, Langmuir 27 (2011) 6701–6711, https://doi.org/10.1021/la2007809.
[49] K. Graf, M. Kappl, Physics and chemistry of interfaces, Wiley-VCH (2006).
[50] J.N. Israelachvili, Intermolecular and Surface Forces, Academic Press, 2011.
[51] C.D.F. Honig, W.A. Ducker, Thin film lubrication for large colloidal particles: experimental test of the no-slip boundary condition, J. Phys. Chem. C 111 (2007) 16300–16312, https://doi.org/10.1021/jp073349i.
[52] L. Bocquet, E. Charlaix, Nanofluidics, from bulk to interfaces, Chem. Soc. Rev. 39 (2010) 1073–1095, https://doi.org/10.1039/b909366b.
[53] B. Ohler, Practical advice on the determination of cantilever spring constants, Bruker Application Note AN94 (2007). http://www.bruker.com.